Biosensors and Bioelectronics 142 (2019) 111567

Contents lists available at ScienceDirect

Biosensors and Bioelectronics

journal homepage: www.elsevier.com/locate/bios

# Dual-readout immunosensor constructed based on brilliant photoelectrochemical and photothermal effect of polymer dots for sensitive detection of sialic acid

Jiani Wang[a,1], Shupei Zhang[b,1], Hong Dai[a,b,*], Hongli Zheng[a], Zhensheng Hong[a], Yanyu Lin[c]

[a] College of Chemistry and Materials Science, Fujian Normal University, Fuzhou, Fujian, 350108, China
[b] Fujian Provincial Maternity and Children Hospital, Fuzhou, Fujian, 350108, China
[c] Fujian Provincial Key Laboratory of Advanced Materials Oriented Chemical Engineering, Fujian Normal University, Fuzhou, Fujian, 350108, China

ARTICLE INFO

*Keywords:*
Dual-readout
Photoelectrochemical
Photothermal
Immunosensor
TPP-Pdots
Salic acid

ABSTRACT

A delicate dual-readout immunosensor based on tetraphenylporphyrin-polymer dots (TPP-Pdots) with brilliant photoelectrochemical and photothermal performance was first successfully fabricated for the ultrasensitive detection of sialic acid (SA). Herein, TPP-Pdots with good biocompatibility, extraordinary light-harvesting ability and excellent photothermal conversion efficiency was used to capture SA antibody as dual-functional bioprobe for generating photocurrent and temperature signal. Furthermore, the large surface and morphology-mediated of rutile-$TiO_2$ (R–$TiO_2$) was beneficial to load amounts of TPP-Pdots for improved PEC signal and photothermal signal. Importantly, the temperature readout resulted from the variation of target concentration could be easily obtained by a universal thermometer which was time-saving and cost-saving. Under the optimized experimental conditions, the photocurrent densities and temperature changes proportionally increased with the increasing of SA concentrations from $3.5 \times 10^{-5}$ ng/mL to 35 ng/mL (R = 0.996). Impressively, the dual-readout approach proposed here not only featured with good accuracy and high sensitivity for SA detection, but also paved the way for the development of a dual-readout immunoassay based on PEC biosensor.

## 1. Introduction

Ovarian cancer had the highest mortality among gynecologic malignancy and it was the fifth most reason of cancer-related deceases among women, which produced more than 150,000 annual deaths in the worldwide (Razmi et al., 2018; Vázquez et al., 2018). Delightedly, the five-year early survival rate significantly increased from 20% in late stage to 90% in early stages (stage I-II) (Shewell et al., 2018). Give the significance of early detection, therefore it was important to find a feasible marker. In this regard, carbohydrate antigen 125 (CA125) and human epididymis protein 4 (HE4) have been usually utilized to monitor patient with ovarian cancer. Unfortunately, several reports suggested that the concentration of these biomarkers would be influenced easily by other elements such as smoking, the abnormal renal function (Ferraro et al., 2015; Zeng et al., 2016). To overcome the above drawbacks, sialic acid (SA), a newly biomarker, presented in human's serum and saliva, which has been pointed by many researches that its elevated concentration was highly relevant to ovarian cancer (Li et al., 2015; Shibata et al., 2012). In addition, it was simple and non-invasive in the process of sample collection that made SA can be extensively employed as a biomarker. Therefore, SA was utilized as a dependable biomarker of ovarian cancer for its early diagnose in this work.

Up to now, several detection methods have been developed to monitor SA such as colorimetric method (Sankoh et al., 2016), electrochemical sensor (Liu et al., 2018), fluorometric assays (Honda et al., 1987), mass spectrometry (Wang et al., 2014), liquid chromatography (Smith et al., 2018). These approaches allowed achieving detect of SA, but all of them were traditional single-readout mode, they were inherently sensitive to interference thus inevitably produced false positive or false negative results. Because of this, they were greatly restricted in actual application for disease diagnosis (Ling et al., 2018; Zhang et al., 2017). Compared with the conventional single-readout analytical protocols, the dual-readout biosensor presented desirable advantages, for instance, improved exactness and more comprehensive information for diagnosis of cancers. The obtained two detection signals could calibrate

* Corresponding author. College of Chemistry and Materials Science, Fujian Normal University, Fuzhou, Fujian, 350108, China.
*E-mail address:* dhong@fjnu.edu.cn (H. Dai).
[1] The author contributed to the work equally and should be regarded as co-first author.

https://doi.org/10.1016/j.bios.2019.111567
Received 18 May 2019; Received in revised form 20 July 2019; Accepted 2 August 2019
Available online 03 August 2019
0956-5663/ 

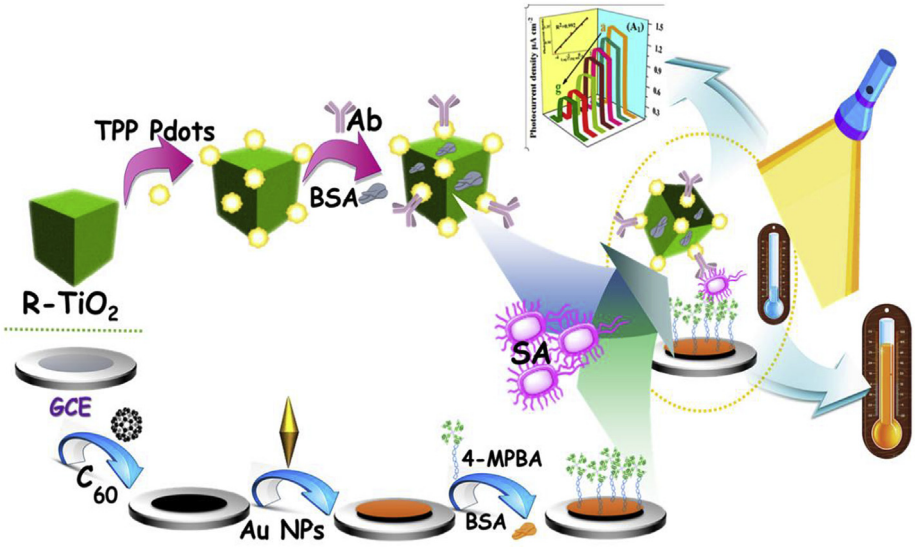


**Scheme 1.**

and support each other roughly, which efficiently avoid producing false positive or false negative results to great extent. Photoelectrochemical (PEC) biosensor has been an innovative and powerful analytical method for biosensing, owing to the inherit merits such as high sensitivity, low background signal, rapid response and simple apparatus (Li et al., 2016b; Xiao et al., 2018). Until now, there were some immunosensors with dual-readout on basis of PEC biosensor were ingeniously designed and sensitively detected several tumor markers (Dai et al., 2016; Gong et al., 2016). Nevertheless, these dual-readout methods unexceptionally possessed complicated signal readout process. Therefore, coupling an easy signal readout sensor with PEC biosensor was favorable to expand its actual application. Photothermal biosensor has drew increasingly intensive interests in the analytical method research due to its inherent superiorities including rapid, simple analytical process and easy signal readout (Lee et al., 2017). Concretely, the temperature changes were closely related to the target concentrations could be obtained conveniently by using a simple thermometer in a photothermal immunosensor. Obviously, the advancement of a photothermal effected-based readout immunosensor widened the application of photothermal effect and enriched point-of-care detection. Motivated by these, a new concise dual-readout biosensor was proposed to improve the accuracy of the determination. In detail, the well-modified electrode was initially irradiated under a 808 nm laser and the temperature measuring equipment was used for monitoring temperature changes resulted from the various concentrations of SA. Subsequently, the cooled electrode with room temperature was tested on electrochemical workstation for obtaining photocurrent signal, which was corresponded to different concentration of SA. This kind of dual-readout biosensor has not been reported to our knowledge.

Undoubtedly, a material integrated photoelectrochemical and photothermal properties played a pivotal part in constructing a dual-readout bioprobe in this work, which avoided the disadvantages based on two individual readout probes including time-consuming, complex-operation even led to undesirable interference. Polymer dots (pdots) was a newly emerged functional nanomaterial has received great attention as a novel semiconductor species in PEC analysis originated from its fantastic optical properties, such as the wide optical absorption range and excellent photostability (Shi et al. 2018a, 2018b). Fortunately, compare with the traditional quantum dots (Qdots) like CdS and CdTe, the pdots presented less cell toxicity and more favorable biocompatibility (Li et al., 2017). Thus it was expected to be a newly photoactive material for constructing PEC biosensor. Furthermore, the pdots exhibited a strong near-infrared absorption and high photothermal conversion efficiency under a 808 nm laser illuminated, which has been successfully applied to photothermal therapy due to its highly effective photothermal performance (Li et al., 2016a). Inspired by these explorations, this work synthesized the Pdots via the nanoreprecipitation method with Poly [(9,9-di-n-octyfluorenyl-2,7-diyl)-alt-(benzo[2,1,3]thiadia-zol-4,8-diyl)] (PFBT), Poly(styrene-co-maleic anhydride) (PSMA) and photosensitizer tetraphenylporphyrin (TPP), which was named as TPP-Pdots for designing a dual-readout bioprobe.

To obtain better analytical performance of the proposed immunoassay, the most efficient method was to employ splendid signal amplification strategy(Zhao et al., 2019). Combing the merits of diverse photoactive species was helpful to ameliorate the photocurrent responses in the previous PEC reports (Soltani et al., 2018; Yu et al., 2019). R–$TiO_2$, a classical photoelectric material, possessed many desirable superiority, for example, excellent photocatalytic activity, large surface, high chemical stability, which has been widely employed in sensitizing solar cell and fabricating PEC biosensor (Fan et al., 2018; Yao et al., 2012). Consequently, R–$TiO_2$ was introduced into this protocol to accumulate more TPP-Pdots, which not only improved the photocurrent density but also enhanced photothermal effect.

Based on the above exploration, a novel dual-readout biosensor based on TPP-Pdots with photoelectric and photothermal property was fabricated for ultrasensitive detecting SA. The prepared process was shown in Scheme 1. Initially, $C_{60}$ and Au nanoparticles (Au NPs) were served as the sensing substrate for improving PEC signal, which attributed to their excellent conductivity for electron transfer. Besides, 4-mercaptophenylboronic acid (4-MPBA) was self-assembled on the surface of the modified electrode via classical Au–S bond for capturing SA due to the biometric recognition between 4-MBPA and SA. Importantly, R–$TiO_2$@TPP-Pdots composite was served as an integrated label for labeling Ab to form R–$TiO_2$@TPP-Pdots@Ab for generating dual-readout signal both photocurrent and temperature signals, which were linearly increased with the increasing concentration of SA. Therefore, a sensitive immunosensor with dual-readout was successfully constructed and commendably accomplished detection of SA, which obtained a credible analytical results and offered a new perspective for analysis of other biomarkers.

## 2. Experimental

### 2.1. Material

Fullerence-$C_{60}$ (99.5% purity) was purchased from New Mater

Nanotecnology Co. Ltd. Hydrogen tetrachloroaurate (III) trihydrate ($HAuCl_4{\cdot}3H_2O$, > 99%), Sodium borohydride ($NaBH_4$, > 96%) and trisodium citrate dihydrate (> 99%) were obtained from Shanghai Sinopharm Chemical Reagent Co. (Shanghai, China). Hexadecyltrimethylammonium bromide (HTAB), 4-Mercaptophenylboronic acid (MPBA), Poly (styrene-co-maleic anhydride) (PSMA) and tetraphenylporphyrin (TPP) were acquired from Aladdin Industrial Co. (Shanghai, China). Poly[(9,9-di-n-octyfluorenyl-2,7-diyl)-alt-(benzo[2,1,3]thiadia-zol-4,8-diyl)] (PFBT) was purchased from Xi'an polymer Light Technology Crop. Tetrahydrofuran (THF) was supplied by Sinopharm Chemical Reagant Co., Ltd. N-hydroxy succinimide (NHS) and 1-ethyl-3-(3-di-methylaminopropyl) carbodiimide hydrochloride (EDC) were obtained from Shanghai Medpep Co. (Shanghai, China). Bovine serum albumin (BSA, 1%) was purchased from Biss Inc. (Beijing, China). SA standard and SA antibody were got from Chundubio (Wuhan, China). Alpha fetoprotein (AFP) were acquired from Beijing biosynthesis biotechnology Co, Ltd. Lentiviral plasmids (LSR) was purchased from Shanghai Genechem Co., LTD. Phosphate buffer solution (PBS) at various pH values were prepared by mixing 0.1 M $Na_2HPO_4$ and 0.1 M $NaH_2PO_4$ under monitoring of PHS-3C exact digital pH metre (Shanghai, China). All other chemical reagents were analytical reagent grand, and didn't need further purified. Deionized water was used throughout this experiment.

### 2.2. Apparatus

The PEC tests were measured on DyneChem Electrochemical workstation (China) with a three-electrode system: a modified glass carbon electrode (d = 3 mm) as the working electrode, a Pt wire as counter electrode, and a saturated Ag/AgCl electrode as the reference electrode. The excitation light was a LED lamp of 450 nm. The 808 nm laser (LSR-PS-II) was purchased from Yuanming Laser Technology Co., (Zhejiang, China). Electrochemical impedance spectroscopy (EIS) experiments were performed on CHI660C electrochemical workstation (Shanghai Chenhua Instrument Co., Shanghai, China). The ultraviolet–visible absorption was conducted on UV 1900 (Shanghai, Lengguang Tech). Fluorescence spectrum was measured on the device originated from Zolix Instrument Co., Ltd. Scanning electron microscopy (SEM, S-4800 instrument) and transmission electron microscopy (TEM, FEI F20 S-TWIN instrument) were used for characterizing the morphologies of the prepared nanomaterials.

### 2.3. Synthesis of R–$TiO_2$

The preparation process of R–$TiO_2$ was according to the previous report with small modification (Hong et al., 2016). Briefly, 3.0 mL titanium (IV) isopropoxide (TIP) was added into 100 mL of 2.2 M HCl solution and kept stirring at 80 °C for 48 h. Afterwards, the obtained white product was centrifuged, washed with deionized water and ethanol to remove the residual inorganic ions and then dried at 60 °C for 10 h.

### 2.4. Preparation of TPP-Pdots

The TPP-doped PFBT nanoparticles were synthesized by re-precipitation method as the previously reported (Li et al., 2017). The PFBT polymer, functional polymer PSMA and TPP were dissolved in THF respectively. Mixing the above solution, a PFBT concentration of 200 μg/mL, a PSMA concentration of 40 μg/mL, a TPP concentration of 10 μg/mL. Then the mixed solution was sonicated for 20 min to form homogenous solution. 4 mL of the above solution was quickly added into 20 mL deionized water in a bath sonicator. Afterwards, THF was removed by nitrogen and was filtered with a 0.22 μm filter. The obtained solution was concentrated by rotary evaporation at 55 °C. Finally, a transparent yellow liquid was obtained and indicated successful synthesis of the TPP-doped PFBT nanoparticles.

### 2.5. Preparation of R–$TiO_2$@TPP-pdots composite

Briefly, 500 μL R–$TiO_2$ (5 mg/mL) and 500 μL TPP-Pdots (5 mg/mL) mixed together at room temperature and shook for self-assembling for 4 h. Afterward, the mixture was centrifuged and washed with deionized water for three times to remove the unabsorbed TPP-Pdots. Finally, the obtained composites were redispersed in deionized water with a concentration of 5 mg/mL.

### 2.6. Synthesis of R–$TiO_2$@TPP-Pdots@Ab bioconjugates

50 μL EDC/NHS (2:1) was added to 200 μL R–$TiO_2$@TPP-Pdot composite (5 mg/mL) to active the carboxyl group of TPP-Pdots for further reaction. 200 μL Ab solution (50 μg/mL) was dropped into the activated solution under stirring and incubated for 40 min at 4 °C. During the process, Ab was successfully attached on the R–$TiO_2$@TPP-Pdots via classical amidation reaction between carboxyl of the composite and amino of Ab. After centrifugation and washing for three times to remove the unbound residue, the bioconjugates R–$TiO_2$@TPP-Pdots@Ab was obtained and then redispersed in 1 mL of PBS.

### 2.7. Fabrication of the dual-readout biosensor

The surface of glass carbon electrode (GCE, d = 3 mm) was polished with 0.3 μm and 0.05 μm alumina powder to obtain a mirror, followed by washing with deionized water. After that, 3 μL $C_{60}$ (3 mg/mL) was coated on the surface of polished GCE and dried under an infrared lamp. Successively, the treated electrode was modified with 3 μL Au NPs in the same way. The resultant electrode was modified with MPBA via Au–S bond. Afterwards, the electrode was incubated with various concentration of SA for 40 min and then washed with deionized water for removing the redundant SA. Lastly, 3 μL R–$TiO_2$@TPP-Pdots@Ab was coated on the pretreated electrode via specific recognization for 40 min and then stored in refrigerator for further use.

## 3. Result and discussion

### 3.1. Characterization of TPP-Pdots and R–$TiO_2$

The particle size and morphology of the prepared TPP-Pdots were displayed in Fig. 1A. From the characterization of TEM, the uniform morphology of quasi-spherical particles with the average diameter of about 5 nm was observed, which was propitious to construct uniform photoresponsive film and generate steady photocurrent signals. Besides, amounts of bundle-like product with about one hundred nanometers were exhibited in Fig. 1B. Surprisingly, the bundle-like product were connected and interlaced with each other, which was beneficial to the transport of photo-induced carries. Evidently, the inset of Fig. 1B displayed the single bundle was composed of tiny bundle subunits.

The normalized absorption emission and photos (inset) of the as-prepared TPP-Pdots were perfectly presented in the Fig. 2. The TPP-Pdots exhibited two obvious absorption in the range of 400–500 nm

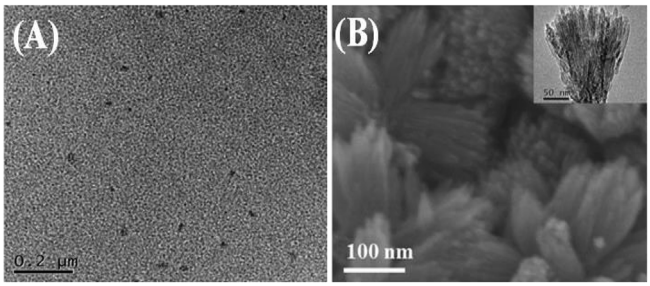


**Fig. 1.** (A) Transmission electron microscope of prepared TPP-Pdots. (B) Scanning electron microscopy of R–$TiO_2$ (inset: TEM).

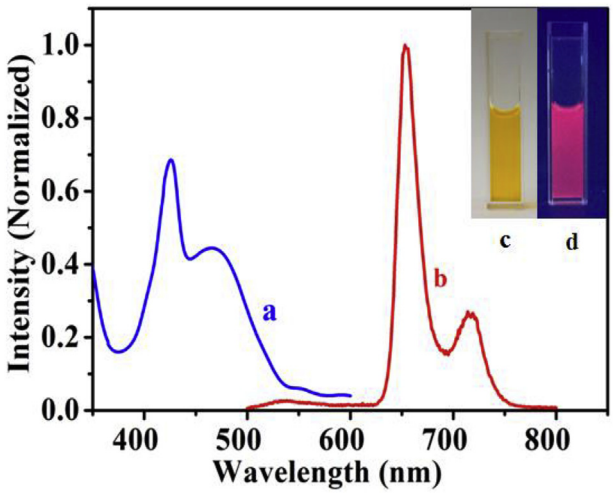


**Fig. 2.** The normalized absorption (a) and emission spctra (b) of the as-fabricated TPP-Pdots, visible photograph (c)and fluorescence image of TPP-Pdots under a 365 UV-lamp (d).

(curve a), the relatively weaker absorption was ascribed to the TPP dopants. The strong absorption in the spectrum revealed the strong light-harvesting property of TPP-Pdots, which enabled it can be employed as a splendid photoactive species to obtain high and steady PEC signals. The fluorescence of TPP-Pdots was measured from 200 nm to 800 nm under the 450 nm excitation as shown in curve b, the strong emission at 660 nm and its shoulder peak at 720 nm were assigned to the characteristic emission of TPP, and the small emission peak at 540 nm was attributed to the pure PFBT polymer, which was quenched by TPP based on the effect of excitation energy transfer (Li et al., 2017). The embedded in the Fig. 2 were the digital and fluorescence images, it could be observed that after the excitation of a 365 nm UV lamp, the color of the solution changed from yellow to red. All the above indicated that the successful synthesis of TPP-Pdots.

### 3.2. Excellent PEC performance of R–$TiO_2$@TPP-pdots

In a typical PEC biosensing device, it is critical to design a suitable platform with less $e^-$–$h^+$ recombination and improved photocurrent, the sensitization effect originated from TPP-Pdots was investigated as shown in Fig. 3. Firstly, open circuit potential (Voc) was evaluated to explore the charge separation efficiency of R–$TiO_2$ and R–$TiO_2$@TPP-Pdots in Fig. 3A. Once the irradiation stopped, the photoelectrons were recombined with photo-generated holes and scavenged by electron acceptor species in electrolyte (Song et al., 2008). The slower decay of the R–$TiO_2$@TPP-Pdots modified electrode indicated that higher charge separation and less recombination in the complex.

Furthermore, comparing the Voc decay measurement between R–$TiO_2$ and R–$TiO_2$@TPP-Pdots after the light was stopped, the lower electron recombination kinetic and the prolonged decay lifetime of R–$TiO_2$@TPP-Pdots could be observed in Fig. 3B. The decay lifetime of the accumulated electron could be obtained by this equation(Dai et al., 2017)

$$\tau = \frac{K_B T}{e}\left(\frac{dVoc}{dt}\right)^{-1} \quad (1)$$

Where τ was the potential dependent lifetime, e was the charge of an electron, $K_B$ was Boltzman's constant, T was the temperature, the dVoc/dt was the derivative of open-circuit voltage transient. Obviously, the complex decreased recombination efficiency and lengthened the photoelectron lifetime.

In addition, to obtain accurate and sensitive detection signal, fabricating an elegant and efficient bioprobe was pivotal. Fig. 3C displayed the PEC signal response of different modified electrodes under the same UV-lamp irradiating. The photoelectric response of R–$TiO_2$@TPP-Pdots (curve b) was significantly higher than R–$TiO_2$ (curve a) in this experiment, which was attributed to the high photoelectric response and efficient charge separation in TPP-Pdots (Shi et al., 2018b). This result revealed that utilizing R–$TiO_2$@TPP-Pdots for labeling SA antibody was more feasible in the analytical application.

Finally, to further evaluate the merits of R–$TiO_2$@TPP-Pdots, the linear sweep voltage experiment was also performed as shown in Fig. 3D. The photocurrent densities of R–$TiO_2$@TPP-Pdots (curve b) and R–$TiO_2$ (curve a) were compared under the chopped light irradiation. Obviously, curve b exhibited a larger photocurrent signal under applied potentials from 0.2 to 0.6 V vs Ag/AgCl at a scan rate of 3 mV/s. All above experiments suggested that TPP-Pdots was an admirable PEC sensitizer for promoting photoelectric conversion efficiency of R–$TiO_2$.

### 3.3. The photothermal performance of the modified electrode

In terms of comparing the photothermal conversion efficiency, Fig. 4A exhibited the temperature variations profiles of different modified electrodes under the 808 nm NIR lamp irradiating. As could be observed, the bare GCE (curve a) showed a negligible temperature change compared with other modified electrode. After modifying with R–$TiO_2$ (curve b), the temperature change improved slightly. Under the identical irradiation, TPP-Pdots/GCE (curve c) showed a remarkable change in temperature, which indicated an intensive NIR-absorbing ability and excellent photothermal effect of TPP-Pdots. Fantastically, coupling R–$TiO_2$ and TPP-Pdots (curve d) led to the highest enhancement in temperature, demonstrating the synergetic effect in photothermal conversion in the composite. Thus it was reasonable to utilize R–$TiO_2$@TPP-Pdot to construct the photothermal bioprobe.

Moreover, to further evaluate the photothermal stability of R–$TiO_2$@TPP-Pdots modified electrode, it was exposed under the cyclic laser irradiating (laser on and laser off) for temperature monitoring. As shown in Fig. 4B, the temperature maintained largely constant after three repeated irradiation cycles, thus proved its excellent photothermal stability for the proposed biosensor. These above results demonstrated that R–$TiO_2$@TPP-Pdots could be used as an excellent photothermal agent, which possessed high photothermal conversion efficiency and stability.

### 3.4. Fabrication procedure of dual-readout biosensor

The construction processes of this proposed immunosensor were monitored by means of comparing the transient photocurrent responses and the temperature variations. It can be observed from Fig. 5A and Fig. 5B, there were negligible photocurrent densities (curve a-e) and no obvious variation in temperature (column a-e) before R–$TiO_2$@TPP-Pdots@Ab anchoring on the interface of the treated electrode through the specific biorecognition between SA and its antibody. Nevertheless, the strong improvement of photocurrent (curve f) and significant temperature change (column f) could be obtained when the bioprobe was captured due to its excellent PEC performance and brilliant photothermal conversion efficiency. These experiment results not only proved the successful construction processes of the biosensor but also reflected the reasonability of this analytical strategy.

To further characterize the successful fabrication procedure of the biosensor, electrochemical impedance spectroscopy (EIS) method, an effective strategy for characterizing the electrochemical conductivity of electrode interface, was performed in Fig. 5C. The electron-transfer resistance (Ret) equaled the diameter of each semicircle, which vividly reflected the electron transfer resistance of redox probe arriving interface of electrode. In the Nyquist diagram, the $C_{60}$/GCE (curve b) exhibited a slightly bigger arc radius than bare GCE (curve a), which ascribed to the excellent conductivity of $C_{60}$. With the Au NPs was coated on, the Au NPs/$C_{60}$/GCE (curve c) presented substantially much

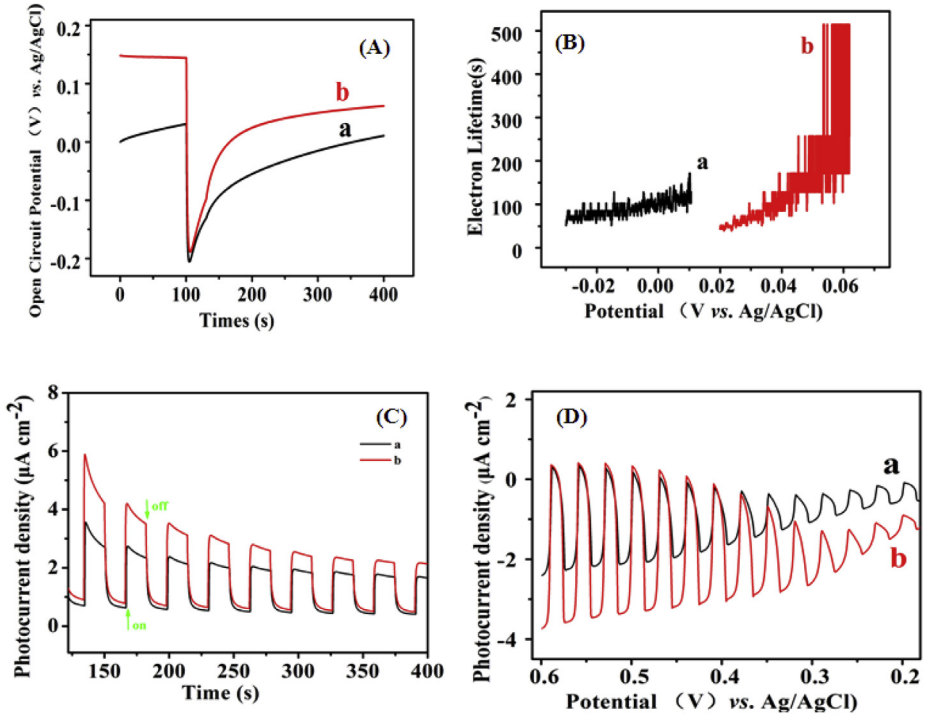


**Fig. 3.** (A) open-circuit voltage response densities. (B) Electron lifetimes measurements (determined from the Voc decay in dark). (C) Photocurrent densities response and. (D) Applied potential bias-dependent photocurrent of (a) R–$TiO_2$ and (b) R–$TiO_2$@TPP-Pdots in 0.1 M PBS (pH 7.0).

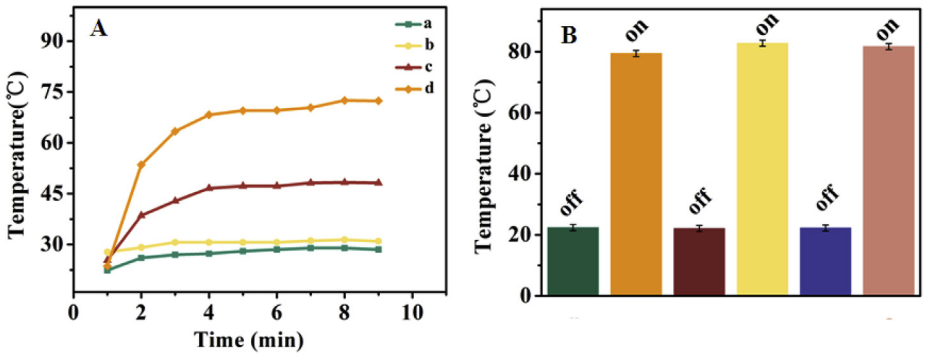


**Fig. 4.** (A) Photothermal effect based on different substrate (a:bare GCE, b:R–$TiO_2$/GCE, c:TPP-Pdots/GCE, d:R–$TiO_2$@TPP-Pdots/GCE) were irradiated by 808 nm laser. (B) The temperature of the electrode modified with R–$TiO_2$@TPP-Pdots under the laser switched on and off for three cycles.

smaller semicircles, suggesting the excellent interfacial charge transfer due to the fact that Au NPS was an admirable electric conducting material. During the following procedure, the bigger semicircle (curve d) was observed after deposition of MPBA, certified the successful assemble via Au–S bond. After the SA was captured on the electrode based on reaction between boronate functional group and SA, the diameter (curve e) increased remarkably, resulting from weak conductivity and insulting property of protein, which impeded the

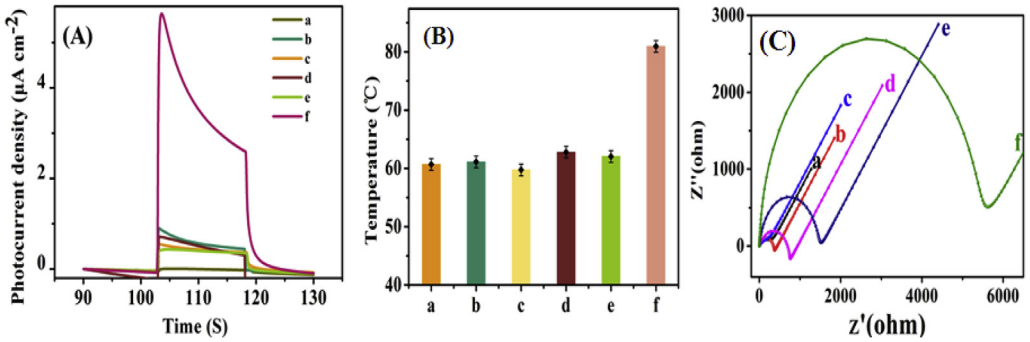


**Fig. 5.** (A) Photocurrent densities response. (B) Photothermal effect. (C) EIS spectra of modified electrode (a) GCE, (b) $C_{60}$/GCE, (c) Au NPs/$C_{60}$/GCE, (d) MPBA/Au NPs/$C_{60}$/GCE, (e) SA/MPBA/Au NPs/$C_{60}$/GCE, (f) R–$TiO_2$@TPP-Pdots@Ab/SA/MPBA/Au NPs/$C_{60}$/GCE.

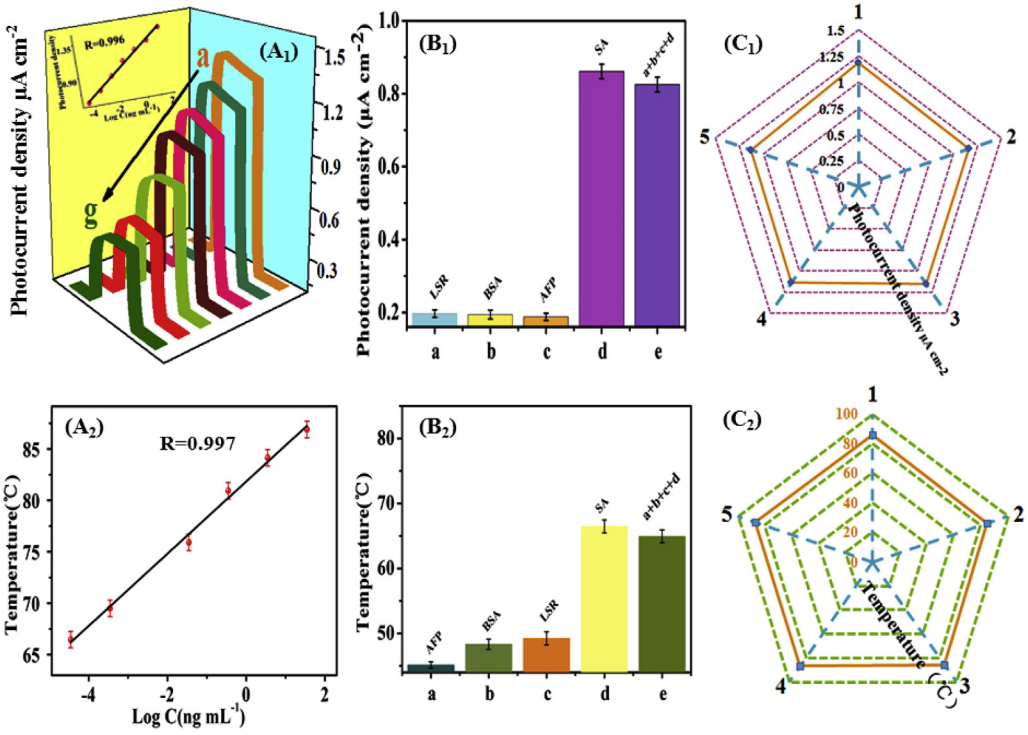


**Fig. 6.** ($A_1$) Photocurrent density, ($A_2$) temperature of different modified electrode incubated with various concentrations (a–g) $3.5 \times 10^{-5}$-35 ng/mL of sialic acids (insert in $A_1$: the corresponding calibration curve). The selectivity of PEC immunoassay ($B_1$) and Photothermal biosensor ($B_2$). ($C_1$) and ($C_2$) were the corresponding stability.

diffusion of redox probe. Finally, the electrode SA/MPBA/Au NPs/$C_{60}$/GCE was incubated with the R–$TiO_2$@TPP-Pdots@Ab bioprobe solution, the Ret (curve f) increased significantly due to the specific biorecognition that induced special steric effect by the bioconjugates. Investigating the each modification step through the resistance changes proved that the successful construction of the dual-readout biosensor.

### 3.5. Analytical performance of the dual-readout biosensor

To acquire the best performance of the bioassay, several crucial experimental parameters such as incubation time, assemble time and the amounts of material were optimized (as shown in Fig. S1). Under the optimum experimental conditions, different standards concentration of SA was sensitively detected by this immunoassay with dual-readout. As expected, the photocurrent densities increased with the increasing of SA concentration and exhibited a well linear relationship with the logarithm of SA from $3.5 \times 10^{-5}$ ng/mL to 35 ng/mL (R = 0.996) and the detection limit was $1.2 \times 10^{-5}$ ng/mL in the Fig. 6$A_1$. Thus the concentration of SA could be well detected by the changes of photocurrent densities. Meanwhile, thermal analysis was achieved by recording the temperature variation with various concentration of SA under the laser irradiation (808 nm, 1.0 w/$cm^2$) as presented in Fig. 6$A_2$. The temperature increased gradually along with the increasing of SA concentration from $3.5 \times 10^{-5}$ ng/mL to 35 ng/mL (R = 0.997) owing to the increasing of the absorbed bioprobe. The recognized bioprobe with excellent photothermal effect under a laser irradiation, the variation of temperature could be monitored through a simple thermometer. Appreciatively, the dual readout biosensor exhibited a wider detection range and lower detection range than the previous reports (Table S1).

Selectivity was another important indicator for analysis application of the proposed dual-readout immunosensor, which was usually investigated by other potential interference. In his work, the pretreated electrode was incubated with other potential protein including LSR, BSA and AFP with ten times concentration than SA concentration, as well as SA and their mixture. Obviously, they not triggered apparent disturbance for PEC and temperature detection in Fig. 6$B_1$ and Fig. 6$B_2$, which suggested good specific recognition and favorable selectivity of the proposed sensor. To further explore the analytical performance of designed platform, the stability of photocurrent and temperature were evaluated for five tests in in Fig. 6$C_1$ and Fig. 6$C_2$. There was no obvious change in detection signal, which indicated the good stability of the immunoassay. These experimental results revealed that the designed dual-readout immunosensor was promising for practical application.

### 3.6. Real sample analysis

In order to prove the designed dual-readout immunosensor was promising for practical application, standard addition method was adopted in this experiment. The human serum from healthy human was diluted with PBS (7.4) for 20 times, three different standard SA solutions were added into the sample as shown in Table 1. The average recovery exhibited acceptable outcomes in the range from 89.7 to 111.4%, implying that the proposed dual-readout biosensor could be used for SA detection in serum sample and opened a new avenue to construct dual-readout immunoassay for ultrasensitive detection.

## 4. Conclusion

In summary, a novel photoelectrochemical and photothermal dual-readout biosensor for SA ultrasensitive detection was successfully proposed based on the brilliant PEC and photothermal properties of TPP-Pdots. Herein, the introduction of R–$TiO_2$ not only accumulated amounts of TPP-Pdots but also sensitized the photocurrent response in this strategy. In addition, the temperature changes induced by the variation of SA concentration could be easily evaluated by a common

**Table 1**
Recoveries tests of SA in real samples (n = 3) [a].

| Sample | Found (ng/mL) | Add (ng/mL) | found (ng/mL) | Recovery (%) |
|---|---|---|---|---|
| **1** | $9.63 \times 10^{-5}$ | blank | $9.63 \times 10^{-5}$ | – |
| **2** | $9.63 \times 10^{-5}$ | $1.0 \times 10^{-4}$ | $9.8 \times 10^{-5}$ | 98 |
| **3** | $9.63 \times 10^{-5}$ | $2.0 \times 10^{-4}$ | $2.11 \times 10^{-4}$ | 105.5 |
| **4** | $9.63 \times 10^{-5}$ | $3.0 \times 10^{-4}$ | $2.89 \times 10^{-4}$ | 96.7 |

[a] n is the repetitive measurements number.

thermometer, which was a versatile protocol for disease monitoring in the point-of-care. More importantly, two detection signals were acquired in this immunoassay, made the analytical results more convinced than traditional single-readout mode. Accordingly, the experimental results demonstrated that the well-fabricated biosensor exhibited wide linear range, low detection, acceptable reproducibility and high stability, which was promising for the determination of other biomarkers.

## Declaration of competing interest

The authors declare that they have no known competing financial interests or personal relationships that could have appeared to influence the work reported in this paper.

## CRediT authorship contribution statement

**Jiani Wang:** Writing - original draft, Investigation. **Shupei Zhang:** Writing - original draft. **Hong Dai:** Funding acquisition, Methodology, Project administration. **Hongli Zheng:** Writing - review & editing. **Zhensheng Hong:** Data curation. **Yanyu Lin:** Formal analysis.

## Acknowledgment

This project was financially supported by the NSFC (21877012, 21575024), National Science Foundation of Fujian Province (2016J06003, 2017J01620) and Education Department of Fujian Province (JK2016009, FBJG20170186, JA14071) was also greatly acknowledged.

## Appendix A. Supplementary data

Supplementary data to this article can be found online at https://doi.org/10.1016/j.bios.2019.111567.

## References

Dai, H., Gong, L., Zhang, S., Xu, G., Li, Y., Hong, Z., Lin, Y., 2016. Biosens. Bioelectron. 77, 928–935.
Dai, H., Chen, S., Li, Y., Zeng, B., Zhang, S., Hong, Z., Lin, Y., 2017. Biosens. Bioelectron. 92, 687–694.
Fan, Z., Fan, L., Shuang, S., Dong, C., 2018. Talanta 189, 16–23.
Ferraro, S., Schiumarini, D., Panteghini, M., 2015. Clin. Chim. Acta 438, 171–177.
Gong, L., Dai, H., Zhang, S., Lin, Y., 2016. Anal. Chem. 88 (11), 5775–5782.
Honda, S., Iwase, S., Suzuki, S., Kakehi, K., 1987. Anal. Biochem. 160, 455–461.
Hong, Z., Hong, J., Xie, C., Huang, Z., Wei, M., 2016. Electrochim. Acta 202, 203–208.
Lee, S.H., Choi, S., Kwon, K., Bae, N.H., Kwak, B.S., Cho, W.C., Lee, S.J., Jung, H.I., 2017. Sens. Actuators B Chem. 246, 471–476.
Li, P.-l., Zhang, X., Li, T.f., Wang, L.l., Du, L.t., Yang, Y.m., Li, J., Wang, H.y., Zhang, Y., Wang, C.-x., 2015. Clin. Chim. Acta 439, 148–153.
Li, S., Wang, X., Hu, R., Chen, H., Li, M., Wang, J., Wang, Y., Liu, L., Lv, F., Liang, X.-J., Wang, S., 2016a. Chem. Mater. 28 (23), 8669–8675.
Li, Y., Zhang, S., Dai, H., Lin, Y., Zeng, B., Hong, Z., 2016b. J. Electroanal. Chem. 783, 242–249.
Li, Y., Zhang, N., Zhao, W.W., Jiang, D.C., Xu, J.J., Chen, H.Y., 2017. Anal. Chem. 89 (9), 4945–4950.
Ling, X., Shi, R., Zhang, J., Liu, D., Weng, M., Zhang, C., Lu, M., Xie, X., Huang, L., Huang, W., 2018. ACS Sens. 3 (9), 1683–1689.
Liu, T., Fu, B., Chen, J., Yan, Z., Li, K., 2018. Electrochim. Acta 269, 136–143.
Razmi, N., Hasanzadeh, M., 2018. Trac. Trends Anal. Chem. 108, 1–12.
Sankoh, S., Thammakhet, C., Numnuam, A., Limbut, W., Kanatharana, P., Thavarungkul, P., 2016. Biosens. Bioelectron. 85, 743–750.
Shewell, L.K., Wang, J.J., Paton, J.C., Paton, A.W., Day, C.J., Jennings, M.P., 2018. Biochemical and Biophysical Research Communications507. pp. 1–4.
Shi, X.M., Mei, L.P., Zhang, N., Zhao, W.-W., Xu, J.J., Chen, H.-Y., 2018a. Anal. Chem. 90 (14), 8300–8303.
Shi, X.M., Mei, L.P., Wang, Q., Zhao, W.W., Xu, J.J., Chen, H.Y., 2018b. Anal. Chem. 90 (7), 4277–4281.
Shibata, T.K., Matsumura, F., Wang, P., Yu, S., Chou, C.C., Khoo, K.H., Kitayama, K., Akama, T.O., Sugihara, K., Kanayama, N., Kojima Aikawa, K., Seeberger, P.H., Fukuda, M., Suzuki, A., Aoki, D., Fukuda, M.N., 2012. J. Biol. Chem. 287 (9), 6592–6602.
Smith, J., Davey, G., Polomc, K., Rovielloe, F., Bones, J., 2018. J. Chromatogr. A 1566, 32–43.
Soltani, T., Tayyebi, A., Lee, B.K., 2018. Appl. Surf. Sci. 448, 465–473.
Song, X., Wu, J., Tang, M., Qi, B., Yan, M., 2008. J. Phys. Chem. C 112, 19484–19492.
Vázquez, M.A., Mariño, I.P., Blyuss, O., Ryan, A., Gentry Maharaj, A., Kalsi, J., Manchanda, R., Jacobs, I., Menon, U., Zaikin, A., 2018. Biomed. Signal Process. Control 46, 86–93.
Wang, D., Zhou, X., Wang, L., Wang, S., Sun, X.L., 2014. J. Chromatogr. B 944, 75–81.
Xiao, N., Liu, S.G., Mo, S., Yang, Y.Z., Han, L., Ju, Y.J., Li, N.B., Luo, H.Q., 2018. Sens. Actuators B Chem. 273, 1735–1743.
Yao, Y., Li, K., Chen, S., Jia, J., Wang, Y., Wang, H., 2012. Chem. Eng. J. 187, 29–35.
Yu, Y., Huang, Z., Zhou, Y., Zhang, L., Liu, A., Chen, W., Lin, J., Peng, H., 2019. Biosens. Bioelectron. 126, 1–6.
Zeng, Q., Liu, M., Zhou, N., Liu, L., Song, X., 2016. Clin. Chim. Acta 455, 102–106.
Zhang, J., He, L., Zhang, X.Z., Wang, J., Yang, L., Liu, B., Jiang, C., Zhang, Z., 2017. Sens. Actuators B Chem. 253, 839–845.
Zhao, C., Ding, S., 2019. Coord. Chem. Rev. 391, 1–14.